

# CO<sub>2</sub> packing polymorphism under pressure: Mechanism and thermodynamics of the I-III polymorphic transition

Ilaria Gimondi, and Matteo Salvalaglio

Citation: *The Journal of Chemical Physics* **147**, 114502 (2017); doi: 10.1063/1.4993701

View online: <http://dx.doi.org/10.1063/1.4993701>

View Table of Contents: <http://aip.scitation.org/toc/jcp/147/11>

Published by the [American Institute of Physics](#)

---

## Articles you may be interested in

[Entropy based fingerprint for local crystalline order](#)

*The Journal of Chemical Physics* **147**, 114112 (2017); 10.1063/1.4998408

[Crystalline structures of particles interacting through the harmonic-repulsive pair potential](#)

*The Journal of Chemical Physics* **147**, 114503 (2017); 10.1063/1.5002536

[Three-body interactions and the elastic constants of hcp solid <sup>4</sup>He](#)

*The Journal of Chemical Physics* **147**, 114504 (2017); 10.1063/1.4985889

[Communication: Hypothetical ultralow-density ice polymorphs](#)

*The Journal of Chemical Physics* **147**, 091101 (2017); 10.1063/1.4994757

[Communication: A method to compute the transport coefficient of pure fluids diffusing through planar interfaces from equilibrium molecular dynamics simulations](#)

*The Journal of Chemical Physics* **147**, 101102 (2017); 10.1063/1.4997865

[Verlet-like algorithms for Car-Parrinello molecular dynamics with unequal electronic occupations](#)

*The Journal of Chemical Physics* **147**, 114102 (2017); 10.1063/1.4987005

---



**Scilight**

Sharp, quick summaries **illuminating**  
the latest physics research

Sign up for **FREE!**

**AIP**  
Publishing

# CO<sub>2</sub> packing polymorphism under pressure: Mechanism and thermodynamics of the I-III polymorphic transition

Ilaria Gimondi and Matteo Salvalaglio<sup>a)</sup>

Thomas Young Centre and Department of Chemical Engineering, University College London, London WC1E 7JE, United Kingdom

(Received 30 June 2017; accepted 25 August 2017; published online 18 September 2017)

In this work, we describe the thermodynamics and mechanism of CO<sub>2</sub> polymorphic transitions under pressure from form I to form III combining standard molecular dynamics, well-tempered metadynamics, and committer analysis. We find that the phase transformation takes place through a concerted rearrangement of CO<sub>2</sub> molecules, which unfolds via an anisotropic expansion of the CO<sub>2</sub> supercell. Furthermore, at high pressures, we find that defected form I configurations are thermodynamically more stable with respect to form I without structural defects. Our computational approach shows the capability of simultaneously providing an extensive sampling of the configurational space, estimates of the thermodynamic stability, and a suitable description of a complex, collective polymorphic transition mechanism. *Published by AIP Publishing.* [<http://dx.doi.org/10.1063/1.4993701>]

## I. INTRODUCTION

Polymorphism, namely, the possibility that molecular crystals assemble in the solid phase in different crystal lattices, is ubiquitous in nature. The spatial arrangement of molecules is a key in defining mechanical, physical, chemical, and functional properties of materials. Understanding the molecular details of the thermodynamics and mechanisms underlying polymorphism is therefore a key to develop detailed, rational descriptions of many natural and industrial processes.<sup>1–8</sup>

In this direction, a notable effort is put in developing both *ab initio* and enhanced sampling techniques to predict polymorphs of a molecule (in particular, crystal structure prediction (CSP) techniques<sup>3,9–11</sup>), to evaluate their relative stability at finite temperature and pressure, i.e., at conditions relevant for the life-cycle of a solid product, and to study the transition mechanism and kinetics. Among enhanced sampling techniques, metadynamics<sup>5,12–20</sup> (MetaD) and adiabatic free energy dynamics<sup>21–23</sup> (AFED) are employed in the literature to study polymorphism. Indeed, over the years, these techniques have been tested, developed, and compared on benchmark systems and combined with CSP methods. Such studies made a successful step towards the characterisation of the solid phase transition, proving these tools to be powerful in the prediction of new structures and transition pathways as well as of the phase diagram without any *a priori* knowledge.

However, a complete and systematic investigation of polymorphic transitions is still challenging.

In this work, our aim is to exploit state-of-the-art enhanced sampling simulations to investigate the thermodynamics and transition mechanisms at play in polymorphic transitions. To this aim, we combine well-tempered MetaD and committer analysis in order to identify a suitable low-dimensional

description of the transition between two polymorphic phases in collective variable (CV) space. To do so, here we focus our attention on solid CO<sub>2</sub>, more precisely on the *I-III* polymorphic transition that characterises CO<sub>2</sub> *packing polymorphism*. *Packing polymorphism* arises when two solid phases differ in the packing of molecules, which have all the same molecular structure, as opposite to *conformational polymorphism*.<sup>2</sup>

In molecular solid phases, CO<sub>2</sub> molecules maintain their gas phase conformation. To a first, crude, approximation, each molecule can in fact be described as rigid and the bending of the O–C–O 180° angle can be reasonably neglected. Thanks to such limited conformational flexibility, it is as easy as spontaneous to identify each CO<sub>2</sub> molecule with a vector passing through its axis; moreover, the centre of mass corresponds to the carbon atom at every simulation time. As a result, the state of each molecule can be completely characterised by the position of its centre of mass and the vector representing its orientation in space.

Despite its simple molecular structure, CO<sub>2</sub> has a rather complex solid-state phase diagram<sup>24</sup> [partially reported in Fig. 1(a)]. Indeed, at high temperature and pressure, seven different crystal structures have been detected so far, among which many are still debated.<sup>24–42</sup> The first form detected was molecular phase I, also called dry ice, crystallised directly from the melt; phase III followed, obtained through the compression of dry ice; the discovery of a polymeric structure, classified as phase V, attracted more interest to the study of this system, resulting in the identification of two more phases, II and IV. Phases II and IV are currently the object of discussion as different groups hold contrasting views on their nature and role in the transition between molecular and non-molecular phases.<sup>24,26,28–30,33,37,43</sup> Furthermore, an amorphous phase (VI) is also identified, and the existence of molecular form VII as a phase itself is still under investigation [see Fig. 1(a)].

In this work, we study the transition between phases I and III, which are largely accepted and well characterised in the

<sup>a)</sup>Electronic mail: m.salvalaglio@ucl.ac.uk

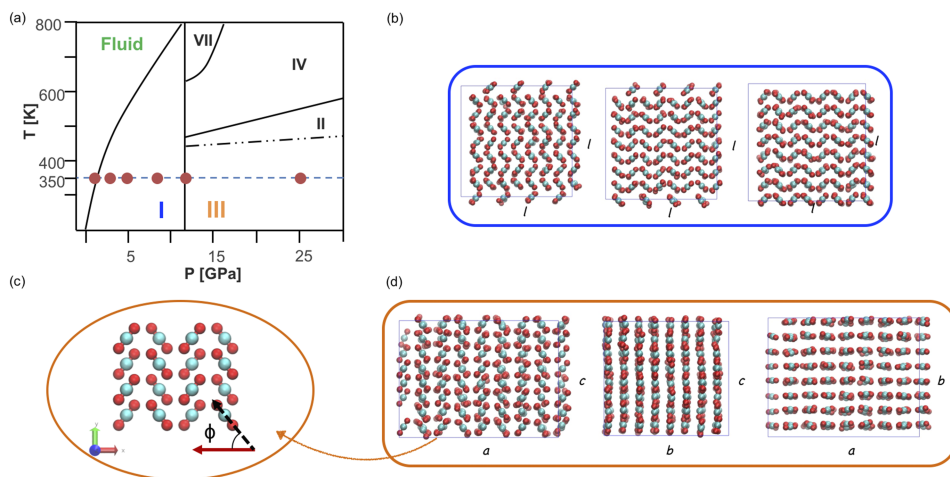


FIG. 1. (a) Details of the phase diagram of CO<sub>2</sub> at high temperature and pressure from the work of Datchi *et al.*<sup>24</sup> with the phases of interest of the present work highlighted (I in blue, III in orange). The red dots represent the condition of temperature and pressure investigated. [(b) and (d)] Snapshots of different planes of the 256-molecule supercell in phases I and III, respectively. (c) Details of phase III with the typical 52-degree angle  $\phi$  are highlighted; in particular, the red arrow aligns with the direction of the side of the box, while the black dashed one aligns with the CO<sub>2</sub> molecular axis.

literature [Figs. 1(b) and 1(d)]. Their structural arrangements appear to hold several similarities. Both polymorphs, indeed, are face centred with four molecules in the unit cell, but while polymorph I's lattice is cubic Pa $\bar{3}$  and III's is orthorhombic *Cmca*. A major difference is the orientation of the CO<sub>2</sub> molecules: in phase I, the molecular axis is in fact aligned with the diagonal of the cell, while in phase III, they are arranged in parallel layers in which molecules describe a characteristic 52° angle,  $\phi$ , with the side of the lattice [Fig. 1(c)].

The I–III transformation takes place at around 11–12 (11.8) GPa<sup>24</sup> independently of temperature ( $\frac{dP_{I\leftrightarrow III}}{dT} = 0$ ); nevertheless, defining the transition conditions is a difficult task, and the pressure transition range is suggested to be wider (7–15 GPa),<sup>35</sup> while Olijnyk *et al.*<sup>44</sup> observed transition III to I under unloading at around 2.5–4.5 GPa at 80 K. There is good agreement on the occurrence of hysteresis of the specific volume, which decreases of about 2% from I to III.<sup>36,37</sup> It is also generally accepted that the transition takes place through a concerted rotation of the molecules together with a deformation of the cubic structure to a parallelepiped, thanks to the peculiar geometrical features of the two phases.

The early studies of Kuchta and Etters<sup>38–40</sup> study such a transition through NPT Monte Carlo (MC) simulations coupled with equalization of the Gibbs free energy in the phases under investigation, not without uncertainties.<sup>40</sup> Moreover, the authors identify the orientation of the molecules in the lattice as the most relevant feature changing in the transition and thus they employ it as a transition coordinate to estimate the free energy profile associated with the transformation; their calculations both at 0 K<sup>38</sup> and room temperature<sup>40</sup> locate the transition pressure at 4.3 GPa. Li *et al.*<sup>41</sup> apply instead the second order Møller-Plesset (MP2) technique to the study of molecular crystals.<sup>42</sup> In their work, they estimate the transition pressure in the 11.9–12.7 GPa range.

Here we aim at complementing the state-of-the-art by uncovering the mechanism of the polymorphic transition between phases I and III. To this aim, we first carry out well-tempered metadynamics simulations<sup>45</sup> at 350 K over a range of pressures to obtain an exhaustive sampling of the configurational space of CO<sub>2</sub> packing. This allows us to consistently sample transition pathways between form I and form III, to identify relevant metastable structures such as

defected configurations, and to estimate their relative thermodynamic stability. We then identify the most probable transition pathway in collective variable space. To assess its reliability, we carry out a committer analysis and a histogram test,<sup>46,47</sup> which allows us to improve the characterisation of the transition pathway and to refine our estimate of the associated free energy barrier.

## II. METHODS

To circumvent time scale limitations of standard molecular dynamics, enhanced sampling techniques are designed to accelerate the sampling of rare events. In this work, we employ well-tempered metadynamics<sup>48</sup> (WTMetaD). Briefly, WTMetaD is based on the introduction of a history-dependent bias potential ( $V_G$ ) along a low-dimensional set of collective variables (CVs).<sup>45,48–51</sup> Such a bias allows for an efficient sampling of phase space, enhancing the escape from long-lived metastable states. Significantly, this result is achieved with little *a priori* knowledge of the free energy landscape and provides an estimate of the unbiased free energy surface [FES,  $F(S)$ ]. For a detailed description of WTMetaD, we refer the interested reader to the studies of Barducci *et al.*,<sup>45,48</sup> and Valsson *et al.*,<sup>51</sup> and for a brief overview of its applications in crystallisation studies, we refer to the work Giberti *et al.*<sup>52</sup>

### A. Force field

Here, we employ the rigid three-site Transferable Potentials for Phase Equilibria (TraPPE) force field<sup>53,54</sup> (Table I), with the Lennard-Jones potential and Lorentz-Berthelot combination rules.

This force field is chosen among a variety of models developed for CO<sub>2</sub><sup>24,26,55,56</sup> since, even if it is not tailor-made for the high temperature and high pressure regime of interest, it outperforms other models in the description not only of the liquid-vapor equilibrium at high pressures<sup>55</sup> (up to 100 MPa) but also of the melting curve of dry ice (up to 1 GPa) and the triple point.<sup>56</sup> Moreover, it has a better representation of the quadrupole, which is indeed relevant in carbon dioxide molecules and plays an important role in the solid phase stabilisation.<sup>57</sup>

TABLE I. Parameters for the TraPPE force field.

$m_C$	$m_O$	$\sigma_{C-C}$ (nm)	$\sigma_{O-O}$ (nm)	$\epsilon_{C-C}$ (kJ/mol)
12	16	0.280	0.305	0.224
$\epsilon_{O-O}$ (kJ/mol)	$q_C$ (e)	$q_O$ (e)	$l_{C-O}$ (Å)	$\alpha_{O-C-O}$ (deg)
0.657	0.70	-0.35	1.160	180

We employ two dummy atoms per molecule<sup>58</sup> to maintain the desired rigidity and linearity of CO<sub>2</sub>, avoiding instability caused by the rigid 180° OCO angle. The most relevant limitation of this model might be the rigidity of the CO<sub>2</sub> molecules.<sup>41</sup>

## B. Simulation setup

Long-range corrections for the van der Waals interactions are included through the *particle mesh Ewald* (*pme*) method. From consistency checks on the effect of the cutoff value on the system volume and energy when treated with *pme*, we find that 0.7 nm provides a good trade-off between accuracy and computational cost.

Isothermal and isobaric (NPT) simulations use a Bussi-Donadio-Parrinello thermostat<sup>59</sup> and a Berendsen anisotropic barostat<sup>60</sup> for T and P control, respectively. The time step employed is 0.5 fs.

For WTMetaD, the initial height of the Gaussians is 10 kJ/mol, with width  $7.81 \times 10^{-3}$  for both CVs. The bias factor is either 100 or 200 to allow the exploration of a wide portion of the phase-space. Moreover, we limit the elongation of each box side from 1.7 to 3.0 nm through the introduction of a repulsive potential. This action prevents an excessive and irreversible distortion of the box when the transition to the melt is observed under anisotropic control. We highlight that such restraints are active only when the system undergoes large fluctuations in the liquid state. The T-P conditions investigated include areas of the phase diagram where the most stable phase changes from the melt to phases I to III. At 350 K, the range of pressure investigated ranges from 1 to 25 GPa (1, 3, 5, 8, 12, 25 GPa). The initial configuration of WTMetaD simulations is phase I, initially equilibrated for 500 ps at NVT, then 5 ns NPT without *pme*, and additionally 5 ns NPT with *pme*. All simulation boxes contain supercells of 256 CO<sub>2</sub> molecules.

We perform MD and WTMetaD simulations with Gromacs 5.2.1<sup>61</sup> and Plumed 2.2,<sup>62</sup> the building of the cells and the post processing of the data employs mainly Visual Molecular Dynamics (VMD),<sup>63</sup> to visualise trajectories, and MATLAB (R2015a).

## C. Committor analysis

As mentioned in the opening, we complement our WTMetaD simulations with a committor analysis. While for a detailed description, we refer to the studies of Tuckerman<sup>47</sup> and Peters,<sup>46</sup> we recall here some useful definitions and procedures.

The committor is defined as the probability  $p_B(r_1, \dots, r_N) \equiv p_B(\mathbf{r})$  that a trajectory initiated from a configuration

$r_1, \dots, r_N \equiv \mathbf{r}$  with velocities sampled from a Maxwell-Boltzmann distribution will arrive in state *B* before state *A*.<sup>47</sup> In our study, we identify *A* as phase I and *B* as III. An important point on the pathway connecting two basins is the transition state (TS, indicated with \*), which is the ensemble of configurations  $\mathbf{r}$  with CV  $\mathbf{S}(\mathbf{r}) = \mathbf{S}^*$  that have committor  $p_B(\mathbf{r}) = 0.5$ ; on free energy hypersurfaces, it corresponds to a saddle point, i.e., the highest energy state along the minimum energy path connecting two basins.

To locate the saddle point, we extract 135 configurations along the transition pathway, and for each of them, we run between 10 and 40 unbiased NPT simulations with different initial velocities randomly generated from a Maxwell-Boltzmann distribution. Simulations are stopped when they commit either basin I or III and they are assigned an outcome value of 0 or 1, respectively. The average of the outcome values obtained from the set of trajectories generated for a given configuration provides an estimate of the committor  $p_{III}(\mathbf{r})$  for that configuration.

We have further analyzed the *histogram test*, which, instead, studies the committor distribution,  $P(p_B(\mathbf{r}))$ , which is the probability that a configuration  $\mathbf{r}$  with  $\mathbf{S}(\mathbf{r}) = \mathbf{S}^*$  has committor  $p_B(\mathbf{r}) = p^*$ . The shape of this distribution is a descriptor of the capability of the CVs to represent the transition mechanism: a Gaussian distribution results from good CVs, while a flat or parabolic distribution corresponds to CVs that do not describe adequately the transition state ensemble.

To evaluate the committor probability, we consider 41 configurations with CVs close to the estimated transition state, and for each of them, we evaluate the committor,  $p_{III}^m$ , as previously described, and build the histogram of  $P(p_{III})$ .

## D. Collective variables

In this work, we use a CV developed by Salvalaglio *et al.*<sup>64–66</sup> and employed it also in the work of Giberti *et al.*<sup>67</sup> In particular, every crystal structure has a unique typical local environment around each CO<sub>2</sub> molecule, a fingerprint of the arrangement, and this order parameter, hereafter called  $\lambda$ , exploits this feature to effectively distinguish polymorphs. Indeed,  $\lambda$  describes crystallinity, a global property of the ensemble, as the sum of local contributions,  $\Gamma_i$ ; each  $\Gamma_i$  takes into account both the local density,  $\rho_i$ , within a cutoff,  $r_{cut}$ , around the *i*-th molecule, and the orientation,  $\theta_{ij}$ , with respect to its neighbours [Fig. 2(a)]. The value of  $\lambda$  ranges between 0 and 1, as it expresses the portion of molecules in the system that are ordered according to the geometry of a defined polymorphic structure.

A complete description of the formulation of this parameter is reported in the [supplementary material](#) and the cited literature.

From the characterization of the local order in polymorphs I and III, we can observe and compare peculiarities of the angle distribution of each phase [Figs. 2(b) and 2(c)], useful in the following tuning of CVs. First of all, the arrangements of phases I and III present similarities, as there is overlap between the distributions of two characteristic angles, which are however centred in different values (in around 70.2° and 109.8° for form I, while in around 75.6° and 104.4° for form III).

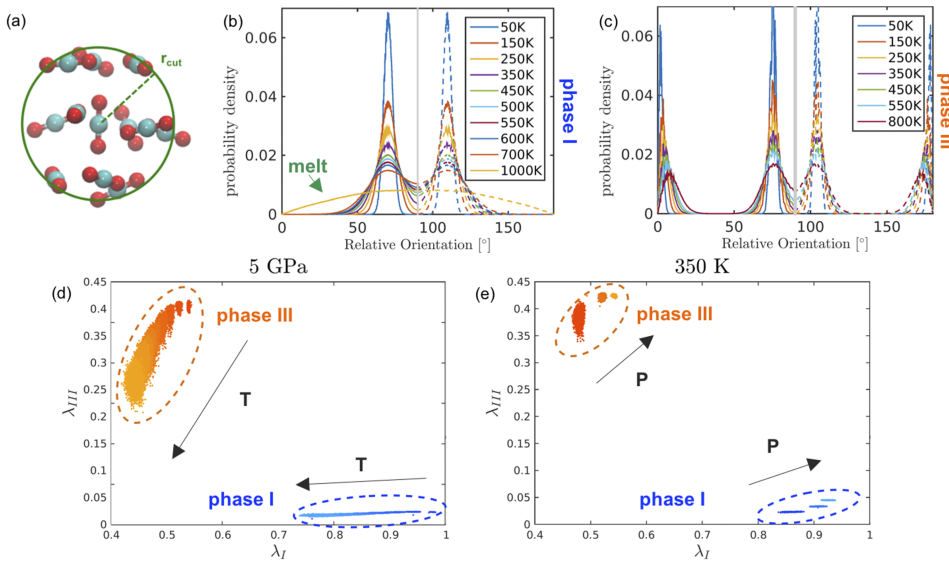


FIG. 2. (a) Visual model of the environment around a CO<sub>2</sub> molecule within the sphere of radius  $r_{cut}$ . [(b) and (c)] Angle distribution over a range of temperature for phases I at 5 GPa (b) and III at 25 GPa (c). The green arrow points an example for the melt. [(d) and (e)] CV-space ( $\lambda_I$ - $\lambda_{III}$ ) for phase I, within the dotted blue line, and phase III, within the dotted orange line at 5 GPa over a range of T from 50 to 1000 K (d) and at 350 K over a range of P from 5 to 25 GPa (e); the arrows point the direction of growing temperature or pressure.

Moreover, phase III populates two additional characteristic angles, with values smaller than  $10^\circ$  and bigger than  $170^\circ$ , which might relate to the presence of layers. We remark also that the melt has a sinusoidal distribution of angles, consistent with a random orientation of molecules. As a final note, increasing temperature enhances the fluctuations of the molecules in the crystal without modifying the mean value of the characteristic angles; an exception to this are the layer angles of form III that, instead, change from  $1^\circ$  to  $8^\circ$  and from  $179^\circ$  to  $172^\circ$  with increasing temperature. The number of neighbours in the first coordination shell shows, instead, a narrow distribution and the same value for the two structures, i.e., 12. Such observations lead to the tuning of two CVs, namely,  $\lambda_I$  and  $\lambda_{III}$  (see [supplementary material](#)).

*Order parameter,  $\lambda_I$* : This CV expresses the degree of phase I-likeness. The purpose of the tuning is to maximize  $\lambda_I$  when the crystal structure is phase I. To reach this aim, two characteristic angles,  $\theta_k$ , are included, which are the ones of phase I (Table II).

*Order parameter,  $\lambda_{III}$* : Similarly, the tuning of  $\lambda_{III}$  aims at maximising the parameter in the presence of phase III. However, in this case, we do not talk about phase III-likeness because as  $\theta_k$  we select only the specific angles that characterize layers (Table II).

For both CVs, the cutoff  $r_{cut}$  is set to  $4.0 \text{ \AA}$ , as it delimits the first coordination shell; the width of the Gaussians associated with the angles,  $\sigma_k$ , instead, is in both cases set to maximise the difference between the value of  $\lambda$  in phase I and the melt and it is the same for both the characteristic angles due to the symmetry (Table II).

TABLE II. Tuning of the  $\lambda$ -order parameters. The angle set,  $\theta_1$  and  $\theta_2$ , and only one Gaussian width, as for symmetry reasons it is the same for both angles, are reported. The cutoff values for the number of neighbours,  $n_{cut}$ , and the coordination shell,  $r_{cut}$ , are presented as well.

	$\theta_1$ (deg)	$\theta_2$ (deg)	$\sigma_1 = \sigma_2$ (deg)	$n_{cut}$	$r_{cut}$ ( $\text{\AA}$ )
$\lambda_I$	70.47	108.86	14.32	5	4
$\lambda_{III}$	8.02	171.89	11.46	5	4

The phase-space evaluated on unbiased MD simulations suggests that the CVs are effective in the distinction of separate and well-defined areas for each phase [Figs. 2(d) and 2(e)]. Furthermore, the average order parameters can be extracted as an ensemble average.

Temperature and pressure act on the location where phases are projected in CV-space: on the one hand, increasing temperature decreases the values of both  $\lambda$ s while widening their fluctuations, consistently with the fact that the volume increases and the molecules vibrate more; on the other hand, increasing pressure leads to an increase in the absolute value of the parameters, while narrowing their distribution.

### III. RESULTS

#### A. Free energy of the I-III polymorphic transition as a function of pressure

In the following, we present the results of our study of the I–III polymorphic transition in CO<sub>2</sub>.

First, we just mention that from preliminary MD unbiased simulations, phase III has a smaller volume than phase I under all conditions investigated ( $\sim 2\%$ , in agreement with experimental results); the volume predictions, however, slightly overestimate the experimental values (Fig. S4 in the [supplementary material](#)). In addition, for the same T-P settings, form I presents a lower potential energy than III: the potential energy of the system is thus not a good indicator of the relative thermodynamic stability at finite temperature. We report the outcome of MD in the [supplementary material](#).

Then, we discuss the results obtained from WTMetaD simulations run with the setup discussed before.

To begin with, we observe the temporal evolution of the CVs, for the explicative case at 350 K, 5 GPa [Figs. 3(a) and 3(b)]; the other conditions investigated (Fig. S5 in the [supplementary material](#)) behave in a reasonably similar way. In the plots in Fig. 3, it is possible to identify the system arranged in phase I as  $\lambda_I$  (a) is high (fluctuations between 0.7 and 0.9) and  $\lambda_{III}$  (b) is below 0.05 and does not present relevant fluctuations, while the box edges (c) have the same length. The

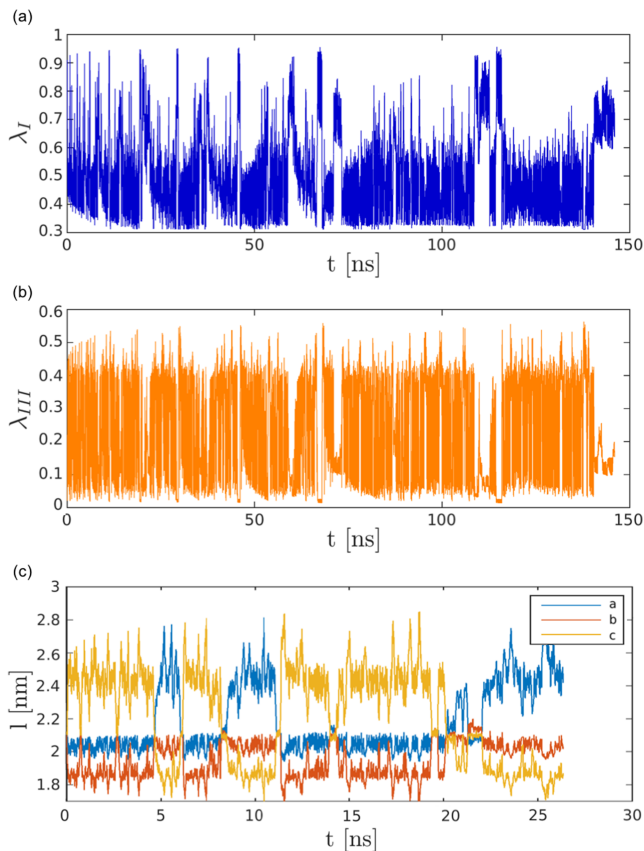


FIG. 3. Time evolution of the CVs  $\lambda_I$  (a) and  $\lambda_{III}$  (b) over 150 ns, and of the box edges (c) for the first 30 ns, of WTMetaD at 350 K, 5 GPa.

exploration of phase III's basin, instead, shows wider fluctuations in the range of 0.36–0.6 for  $\lambda_I$  (a) and 0.1–0.4 for  $\lambda_{III}$  (b); the box edges, moreover, fluctuate around the unbiased average. Thanks to this clarification, it is possible to spot in Fig. 3 that the system undergoes a significant number of recrossings between polymorphs I and III, in particular, four in slightly more than 5 ns at the beginning of the run. In addition, the system explores areas of the CV-space which do not represent any of these polymorphs, feature that will result more evident from the plots of the free energy surface (Fig. 4). On the same surfaces, it will be possible to notice the important role that the mentioned fluctuations of the CVs have on the shape of the basins for the two phases.

Furthermore, by observing the output trajectories and data of WTMetaD, we remark two interesting behaviours: on the one hand, CO<sub>2</sub> molecules in the simulation box rearrange with a concerted motion during a phase transition; on the other hand, we find that such a transition is anisotropic, meaning that each side of the box is equally likely to either elongate or shorten from I to III [Fig. 3(c)]. In particular, this latter observation is important since by biasing as CVs order parameters that account for the spatial orientation of molecules, we obtain the consequential deformation of the supercell, without considering the box volume or edges as CVs, as instead done in previous MetaD works on polymorphism.<sup>5,13–16,18–20</sup>

Next, we present the free energy surfaces (FESs) reconstructed by WTMetaD. In such FESs, the free energy is expressed as a function of the CVs:  $G(\lambda_I, \lambda_{III})$  [Figs. 4(a) and

4(f)–4(i)]. Before proceeding with the discussion, we underline that the FES at 25 GPa is not reported, as no recrossing is sampled from phase III; in addition, the results at 1 GPa are taken into account only qualitatively since under such conditions phase III is so unstable that spontaneously evolves to I in standard MD and it is thus not possible to locate its basin.

Some considerations can be drawn from the study of the FESs. First of all, the location of the minima on the FES for phases I and III is accurately close to the prediction in Figs. 2(d) and 2(e). Moreover, phase III has a much wider basin than phase I and it develops mainly along  $\lambda_{III}$ , while phase I's mainly along  $\lambda_I$ , as underlined for the temporal evolution of the CVs (Fig. 3). As mentioned before, the system explores a wide area of CV-space and, in particular, the presence of black boxes in Fig. 4 highlights the presence of defected phase I structures, which we shall analyze in detail later on. Relevant structural arrangements are reported in Figs. 4(b)–4(e).

In order to compare the results of WTMetaD with the experimental phase diagram, we study quantitatively the relative stability between polymorphs.

Keeping in mind that the free energy is a function of the probability distribution of the CVs, it is possible to evaluate  $\Delta G_{I-III}$  as follows:

$$\Delta G_{I-III} = G_I - G_{III} = -\beta^{-1} \ln \left( \frac{p_{pI}}{p_{pIII}} \right), \quad (1)$$

where  $p_{pI}$  is the probability of phase I,  $p_{pIII}$  is the probability of phase III, and  $\beta$  is  $1/kT$ . The probability of each phase is computed as the integral of the distribution within the basin it occupies on the CV-space,

$$p_{pI} = \int_I p(\lambda) d\lambda = \iint_{\lambda_I, \lambda_{III} \in I} p(\lambda_I, \lambda_{III}) d\lambda_I d\lambda_{III}, \quad (2)$$

$$p_{pIII} = \int_{III} p(\lambda) d\lambda = \iint_{\lambda_I, \lambda_{III} \in III} p(\lambda_I, \lambda_{III}) d\lambda_I d\lambda_{III}. \quad (3)$$

The integration domains are identified by coloured boxes on the FES in Figs. 4(a) and 4(f)–4(i). In Fig. 5(a), we report relevant  $\Delta G$  values over the range of pressure considered. The relative stabilities in Fig. 5(a) together with the FESs in Fig. 4 allow us to draw some considerations on the phase diagram. We observe that while the boundary of the solid-melt transition is in good agreement with experiments, the I–III transition pressure appears to be underestimated. From the  $\Delta G_{I-III}$  pattern shown in green in Fig. 5(a), the transition pressure at 350 K can be estimated as around 4.5 GPa. Despite underestimating the experimental value, the transition pressure agrees with the literature results obtained by treating CO<sub>2</sub> as a rigid molecule.<sup>38–40</sup> We also recall that commonly experimental works rather than a single value report a transition pressure interval (see the Introduction), to which our estimation is closer.

Nevertheless, it is possible to notice that WTMetaD simulations are able to represent the overall trend observed in the phase diagram: increasing pressures increase the stability of phase III, while at decreasing values of pressure, phase I is more stable, ultimately reaching the boundary with the melt.

Since the behaviour of solid carbon dioxide is so well described, it is possible to consider a translation of the phase diagram.

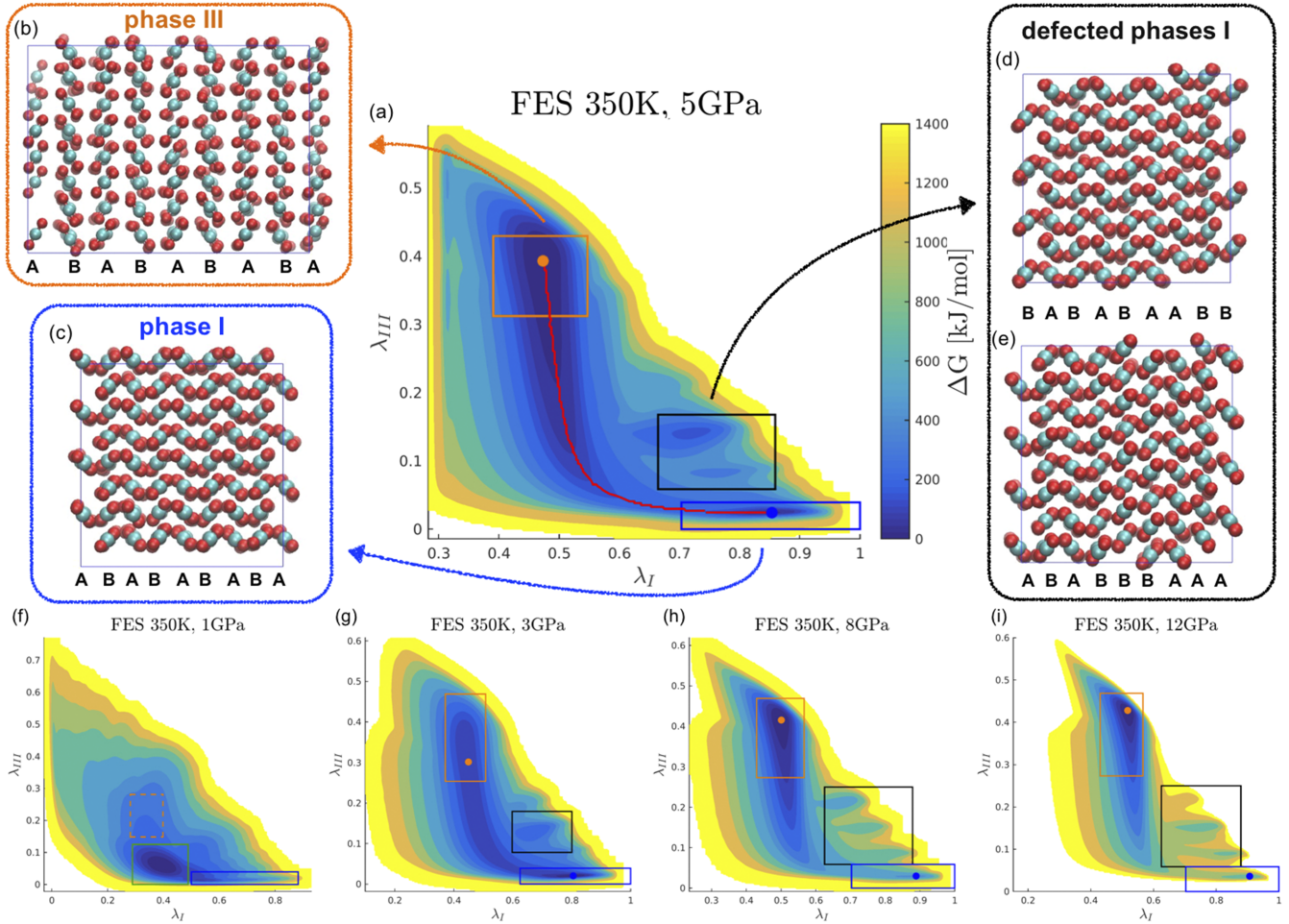


FIG. 4. FESs at 350 K under a range of pressure: 1 GPa (f), 3 GPa (g), 5 GPa (a), 8 GPa (h), and 12 GPa (i). The colour bar spaces for all surfaces from 0 to 1400 kJ/mol. Blue boxes locate the basin of phase I, orange boxes locate the basin of phase III, and the melt is within a green box while black rectangles identify phase I with defects. In addition, (a) reports also the minimum free energy transition path (red). The structures reported are III in (b), I in (c), and two examples of packing faults in (d) and (e); the letters are an aid to compare the packing. Only one plane is displayed as the most explicative of defects; however, while one of the not shown planes is almost perfect, the other has the correct motif, but the layers are not perfectly aligned.

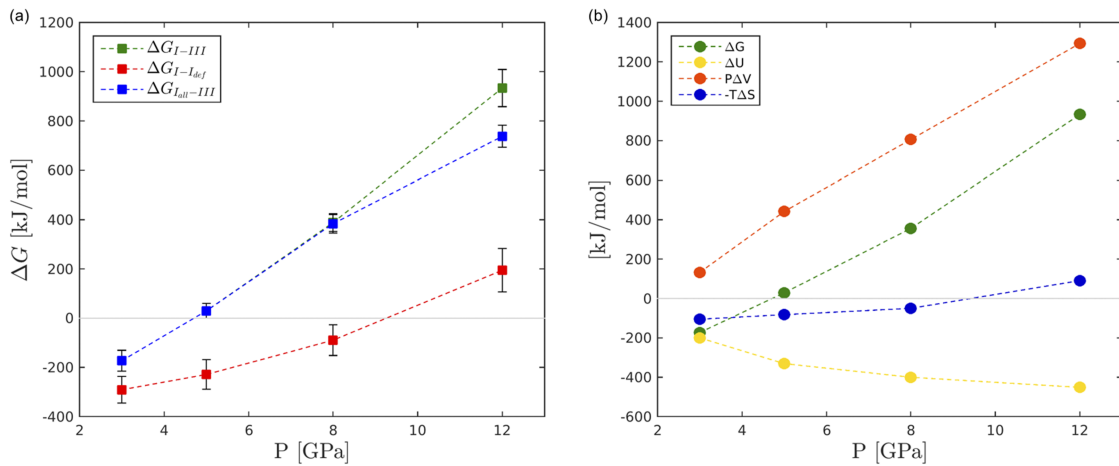


FIG. 5. Relative stability between different phases (a) and breakdown of the free energy (b) at 350 K and increasing pressure from 3 to 12 GPa. In (a), green squares represent  $\Delta G$  between phase I and III, red squares represent  $\Delta G$  between perfect phase I and defected structures I, while blue squares represent  $\Delta G$  between a comprehensive phase I, including configurations with and without defects, and phase III. Positive values of  $\Delta G$  mean that phase III (green, blue) and defected I (red) are more stable. The error bars are obtained from a weighted averaged on simulation time, similar to the work of Berteotti *et al.*<sup>68</sup> In (b), the focus is on the contributions to the relative stability between phases I and III:  $\Delta G$  obtained by WTMetaD is again plotted in green, yellow represents the internal energy difference of the two phases from MD, and red represents their difference in mechanical work from MD, while blue represents the entropy difference obtained from the definition of Gibbs free energy [Eq. (4)]; we report the entropic contribution as  $-T\Delta S$  so that for all the terms considered negative values stabilize phase I and positive phase III. In both graphs, dashed lines are an aid to the eye to visualise the trend.

A further step in the analysis of the I–III relative stability is the breakdown of the free energy in its internal energy, mechanical work, and entropy contributions. With this aim, we first evaluate the difference in internal energy,  $\Delta U$ , and mechanical work,  $P\Delta V$ , between phase I and phase III from the ensemble averages computed from the unbiased MD simulations; the entropy is thus obtained from the macroscopic definition of Gibbs free energy,

$$\Delta G = \Delta U + P\Delta V - T\Delta S. \quad (4)$$

From the results in Fig. 5(b), it is possible to notice some major features. First of all, the internal energy,  $\Delta U$ , stabilizes form I, while  $P\Delta V$  is significant in the stabilisation of phase III; in both cases, their contribution becomes more relevant with growing pressures. The entropic term, instead, tends to favour form I, a part from a pressure of 12 GPa.

### 1. Defected phases

As mentioned in the analysis of the CVs (Fig. 3) and of the FESs (Fig. 4), at pressure equal and above 3 GPa, our simulations allow us to identify additional basins corresponding to structures which are not known *a priori* and correspond to defected phase I configurations [Figs. 4(d) and 4(e)]. Indeed, such structures are similar to phase I, being almost cubic and having a comparable arrangement; however, they display packing faults, *planar defects* that break the orientation motif recognisable in perfect phase I structures. The phase I arrangement presents the repetition of rows of CO<sub>2</sub> that alternate the orientation with respect to the Cartesian axis according to an ABABABAB sequence [Fig. 4(c)], while the defected structures replicate two or more AA or BB motifs [Figs. 4(d) and 4(e)]. To complete the analysis of these configurations, we run unbiased simulations of the defected structures under the same T-P conditions as the corresponding WTMetaD. These trajectories show that defected configurations do not spontaneously undergo any transition, confirming that these configurations are metastable structures and that the appearance and disappearance of defects is an activated event. It should be noted

that close to the form I melting line, defected phase I configurations do not correspond to local minima in the FES [Fig. 4(f)] and do not emerge as metastable intermediates in the melting process which, at 350 K and 1 GPa, resembles a single barrier crossing event rather than a defect-mediated process.<sup>69,70</sup> It is particularly remarkable of the capability of WTMetaD to consistently sample such structures since despite this phenomenon can take place in experiments, it is considered to be under-represented in the current literature.<sup>71</sup> In addition, we note that the stability of the defected configurations increases with pressure, becoming ultimately more stable than phase I without defects at 12 GPa [ $\Delta G$  in red in Fig. 5(a)]. A thorough analysis of this trend is beyond the scope of this paper and we reserve to discuss it in depth in a future study.

### B. Commitor analysis

In the first part of this work, we have shown that our  $\lambda$ -order parameters are effective CVs in sampling the transition between polymorphs I and III, evaluating their relative stability, and exploring the phase space. In the following, we focus instead on the mechanism of the title transition. In particular, such an analysis allows us to evaluate the goodness of the CVs in the representation of the process and to estimate quantitatively the transition pathway and the energy barrier to overcome.

First of all, we characterize the minimum free energy path (MFEP) that connects the free energy minima corresponding to phases I and III. The MFEP provides a representation in CV-space of the most probable set of intermediate states involved in the transition. Furthermore, the free energy profile along this path yields an estimate of the free energy barrier associated with the polymorphic transition. As an initial estimate of the MFEP, we propose an approximation obtained as the combination of the projection of FES along the CVs, more precisely, of basin I along  $\lambda_I$  and of basin III along  $\lambda_{III}$ , due to the observation of typical L-shaped FES; further details about these approximations are provided in the

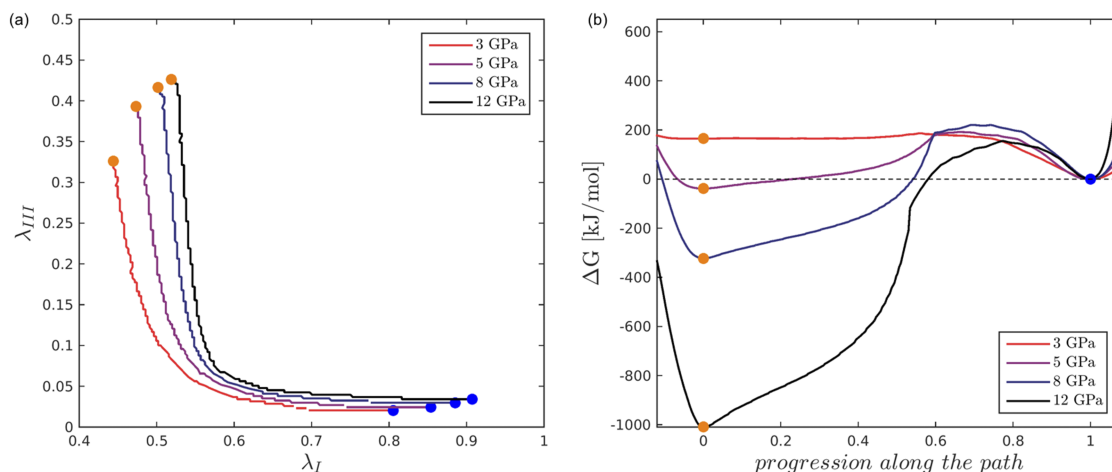


FIG. 6. (a) Transition pathway in the space of CVs at 350 K over the range of pressures investigated. (b) Projection of the free energy along the curvilinear path coordinate at 350 K over a range of pressures. The progression along the MFEP spaces between 0 in phase III and 1 in phase I. The minimum of phase I's basin is the free energy reference. In both graphs, blue dots represent phase I, while orange represent phase III.

supplementary material. We then employ such a path as educated guess for an optimisation routine that enables to obtain the actual MFEP from a series of trial moves, whose acceptance is based on the free energy value. The algorithm is robust

and the path converges to the same route from different and less educated initial guesses.

In Fig. 4(a), we report the MFEP on the FES at 350 K, 5 GPa, while in Fig. 6(a), we compare transition pathways

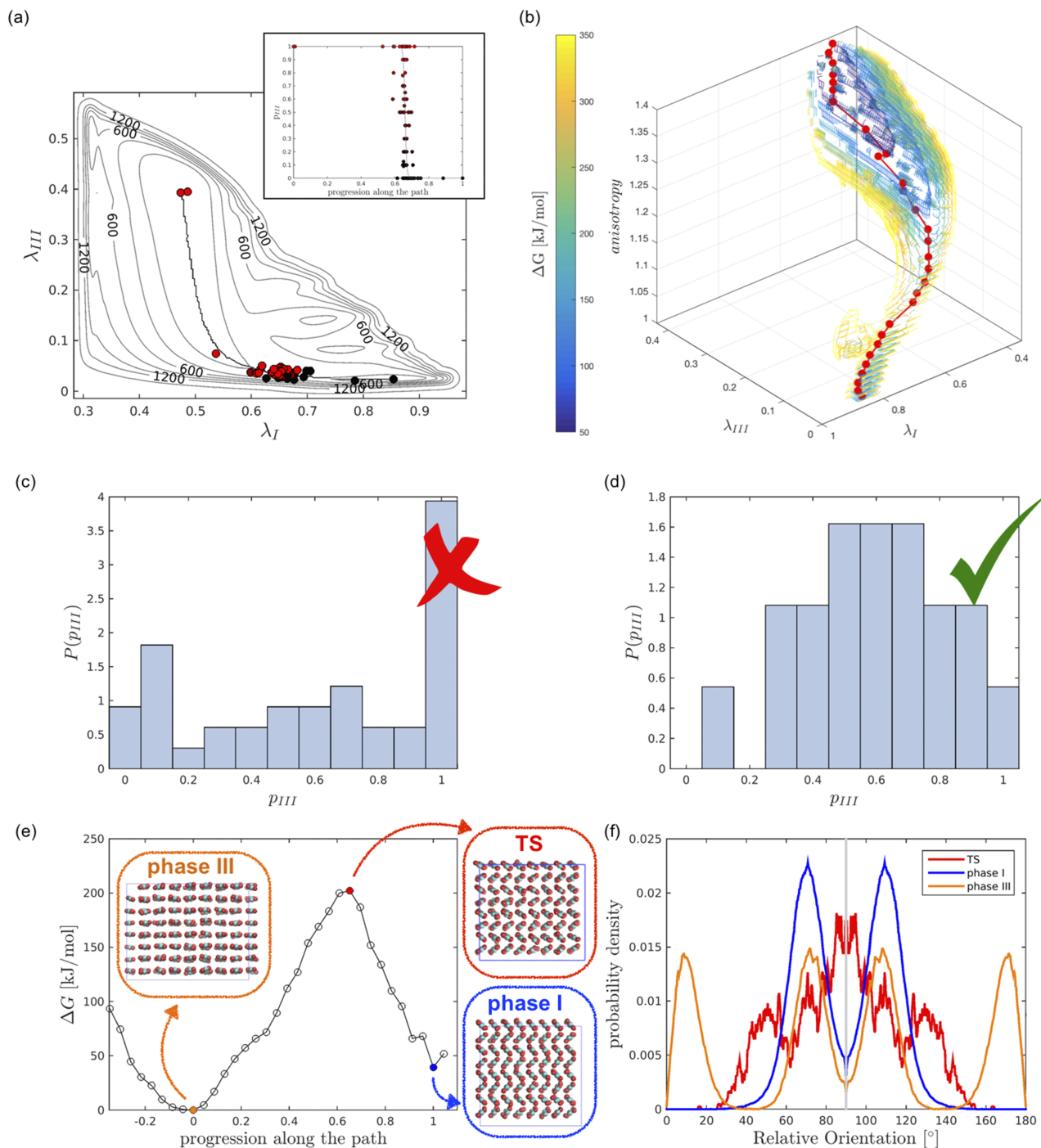


FIG. 7. Committor analysis results, with the transition mechanism described only by the CVs [(a) and (c)] or by the CVs and the box anisotropy [(b) and (d)–(f)]. In (a), coloured dots represent configurations,  $\mathbf{r}$ , extracted along the MFEP (black) on the CV-space; their colour is based on the committor of each configuration, shading from black for  $p_{III}(\mathbf{r}) = 0$  to red for  $p_{III}(\mathbf{r}) = 1$ . The same colour code applies to the inset in (a), which reports the committor as a function of the progression along the MFEP; in the same graph, the sigmoid dashed line is an aid to the eye to read the trend. The histogram test on configurations  $\mathbf{r}$  so that  $\lambda(\mathbf{r}) = \lambda^*$  of the TS shows three peaks (c). The inclusion of the box anisotropy to the  $\lambda$ -order parameters to describe the mechanism requires a 3D representation, and thus in (b), we report the free energy as a function of these three parameters through a colour plot and the transition path through red dots; the results of the histogram test (d) on configurations with the same  $\lambda_I$ ,  $\lambda_{III}$ , and anisotropy of the TS confirm that this set of parameters is effective and complete. In (e), the free energy is plotted as a function of the progression along the 3D path highlighted in (b), with reference in phase III (at progression zero along the path), a blue dot locates phase I (at progression 1), and a red dot locates the transition state; representations of the structures of phase I, phase III, and the TS are within blue, orange, and red rectangles, respectively. The same colour code is employed for the angle distributions for phase I, phase III, and the TS presented in (f).

evaluated at different pressures. Interestingly, pressure only slightly affects the typical L-shape of the transition pathway, with the major difference being the location of the minima. Moreover, at this level of detail, the energy barrier to overcome from phase I to III appears similar at all pressures investigated [Fig. 6(b)]. We also highlight that the MFEP converges much earlier than the simulation, and no alternative routes connecting polymorphs I–III arise (Fig. S7 in the [supplementary material](#)).

The next step towards a quantitative characterization of the transition mechanism is the validation of the MFEP through a committor analysis,<sup>46,47</sup> with a histogram test on the *apparent* transition state. We discuss hereafter the explicative case of 350 K, 5 GPa.

To begin with, we locate the transition state by evaluating the committor of 135 configurations extracted along the MFEP. Interestingly, configurations with the committor different from zero and one are not evenly distributed along the transition pathway, but grouped in a narrow area around the saddle point, estimated in  $\lambda_I^* = 0.65$ ,  $\lambda_{III}^* = 0.034$ ; as a result, the cumulative distribution along the path resembles a steep sigmoid [Fig. 7(a)]. The behaviour shown in Fig. 7(a) suggests that the order parameters alone might not be enough to account for the transition mechanism. The validation proceeds with a histogram test on the saddle point. We evaluate the committor of 41 configurations with  $\lambda(\mathbf{r})$  around  $\lambda^*$  and represent the results on a histogram [Fig. 7(c)]. Such a histogram shows three peaks, a sign that our CVs alone are not effective reaction coordinates and other parameters need to be included in the mechanism description.

In order to identify the additional parameters to take into account, we deepen our analysis and further investigate the dependence of  $p_{III}(\mathbf{r})$  on properties such as potential energy, volume, and box dimensions (Fig. S6 in the [supplementary material](#)). The results suggest that the deformation of the lattice plays a role in the representation of I–III transition mechanism. We define this deformation through the simulation box *anisotropy*, i.e., the ratio between the longest and the shortest sides of the cell; its value spans from 1 in cubic phase I to 1.35 in orthorhombic phase III. As a result, we note that only configurations  $\mathbf{r}$  along the pathway with anisotropy of the box between 1.14 and 1.145 have a committor non-identical to 0 or 1, and, in particular the TS is uniquely located in  $\lambda_I^* = 0.65$ ,  $\lambda_{III}^* = 0.034$ ,  $anisotropy^* = 1.1421$ , while characteristic orientations are presented in Fig. 7(f). We thus repeat the histogram test on 19 configurations with CVs and *anisotropy* close to the TS and the outcome shows, as expected, a Gaussian shape [Fig. 7(d)]: as a result, to effectively describe the mechanism of the I–III transition of solid CO<sub>2</sub>, all three parameters, namely,  $\lambda_I$ ,  $\lambda_{III}$ , and *anisotropy*, have to be taken into account.

We thus evaluate<sup>72</sup> the free energy as a function of the three parameters of interest:  $G(\lambda_I, \lambda_{III}, anisotropy)$ . On such FES, we identify the 3D MFEP that connects phase I to phase III [Fig. 7(b)]: its projection on the  $\lambda_I - \lambda_{III}$  plane reasonably overlaps with the MFEP previously evaluated; moreover, the anisotropy of the box monotonically increases from I to III, and vice versa.

Summing up the analysis carried on in this second part of the work, the transition from cubic phase I to orthorhombic

phase III can be thus described as the sequence of the following actions:

- The CO<sub>2</sub> molecules first tend to distort the typical phase I lattice and, as a consequence, the value of  $\lambda_I$  decreases, with no relevant increase of  $\lambda_{III}$  (horizontal branch of the L-shaped pathway); at the same time, the box starts deforming, elongating one side and reducing the others, thus increasing its anisotropy.
- Then, when the deformation of the cell reaches the anisotropy threshold value of the transition state, the system completes the rearrangement to phase III; indeed, the molecules start organizing into parallel layers and the volume decreases. From this point, the transformation proceeds on the vertical branch of the L-shaped pathway, with increasing  $\lambda_{III}$  for relative small variations of  $\lambda_I$ .

The motion of the molecules in the crystal during the transition is concerted.

From the investigation of the 3D MFEP, we obtain also quantitative information about the height of the barrier for the polymorphic transformation: for a system composed by 256 CO<sub>2</sub> molecules at 350 K, 5 GPa, the transition state is located at about 202 kJ/mol [Fig. 7(e)], with reference zero in phase III, i.e., the absolute minimum of the FES.

#### IV. CONCLUSIONS

In this work, we investigated the I–III transition in CO<sub>2</sub> under pressure by combining molecular dynamics, well-tempered metadynamics, and committor analysis.

First, we performed WTMetaD simulations at 350 K over a range of pressure (1–25 GPa) with two order parameters as CVs. These parameters,  $\lambda_I$  and  $\lambda_{III}$ , are built on the local order around each CO<sub>2</sub> molecule and account for the reorientation of the molecules in the crystal. This feature allows us to clearly distinguish in the  $\lambda_I - \lambda_{III}$  CV space configurations that belong to phase I or phase III and to clearly resolve amorphous configurations. Moreover, metadynamics exploration with these CVs allows us to sample the formation of packing faults in phase I. Interestingly, we observe the deformation of the cell, a *global* rearrangement of the configuration, taking place as a consequence of biasing along variables  $\lambda_I$  and  $\lambda_{III}$ , which account for local order. The rotationally invariant character of these variables also allowed us to sample the I–III transition without defining *a priori* a deformation direction for the simulation box.

From the FESs resulting from WTMetaD, we evaluated the free energy difference between polymorphs; we observed that the predicted trend of the I–III relative stability over pressure is in agreement with the carbon dioxide phase diagram: increasing pressures move from the melt-phase I boundary, to the region of stability of phase I, and to the one phase III. We estimate the transition pressure at  $\sim 4.5$  GPa, in agreement with previous literature studies that considered carbon dioxide as a rigid molecule.<sup>38–40</sup> Furthermore, our model suggests that the stability of the defected configurations increases with pressure. While at low pressures, form I without defects is more

stable than the ensemble of its defected counterparts, and at high pressures, the latter dominate.

Alongside a description of the I-III transition thermodynamics, we assess the I-III polymorphic transition mechanism for the representative case at 350 K, 5 GPa. To this aim, we identify the MFEP connecting phase I to phase III in CV space and we validated the pathway carrying out a committor analysis and a histogram test on an ensemble of configurations corresponding to the saddle point in CV space. From this analysis, it emerges that to quantitatively identify the transition mechanism, we need to consider the anisotropic deformation of the CO<sub>2</sub> supercell alongside the order parameters accounting for the local arrangement of CO<sub>2</sub> molecules. This analysis allowed us to identify a reliable approximation of the transition pathway, to characterise the I-III transition as a concerted distortion process, and to quantify the free energy barrier associated with the transition.

Our work shows that by combining opportunely designed order parameters with state-of-the-art enhanced sampling methods and committor analysis, we can provide an in-depth characterisation of both thermodynamics and transition mechanisms of polymorphic transformations in molecular crystals at finite temperature.

## SUPPLEMENTARY MATERIAL

See [supplementary material](#) for further details on the collective variables and additional results on MFEP, committor analysis, and unbiased simulations.

## ACKNOWLEDGMENTS

The authors acknowledge EPSRC (Engineering and Physical Sciences Research Council) for Ph.D. scholarship and UCL Legion High Performance Computing Facility for access to Legion@UCL and associated support services in the completion of this work.

- <sup>1</sup>A. J. Cruz-Cabeza, S. M. Reutzel-Edens, and J. Bernstein, "Facts and fictions about polymorphism," *Chem. Soc. Rev.* **44**(23), 8619–8635 (2015).
- <sup>2</sup>A. J. Cruz-Cabeza and J. Bernstein, "Conformational polymorphism," *Chem. Rev.* **114**(4), 2170–2191 (2014).
- <sup>3</sup>S. L. Price, "Computational prediction of organic crystal structures and polymorphism," *Int. Rev. Phys. Chem.* **27**, 541–568 (2008).
- <sup>4</sup>S. L. Price, "Crystal energy landscapes for aiding crystal form selection," in *Computational Pharmaceutics* (John Wiley & Sons, Ltd, Chichester, UK, 2015), Chap. 2, pp. 7–29.
- <sup>5</sup>T. Zykova-Timan, P. Raiteri, and M. Parrinello, "Investigating the polymorphism in PR179: A combined crystal structure prediction and metadynamics study," *J. Phys. Chem. B* **112**(42), 13231–13237 (2008).
- <sup>6</sup>O. Valdes-Aguilera and D. C. Neckers, "Aggregation phenomena in xanthene dyes," *Acc. Chem. Res.* **22**(5), 171–177 (1989).
- <sup>7</sup>P. Vishweshwar, J. A. McMahon, M. Oliveira, M. L. Peterson, and M. J. Zaworotko, "The predictably elusive form II of aspirin," *J. Am. Chem. Soc.* **127**(48), 16802–16803 (2005).
- <sup>8</sup>J. Bauer, S. Spanton, R. Henry, J. Quick, W. Dziki, W. Porter, and J. Morris, "Ritonavir: An extraordinary example of conformational polymorphism," *Pharm. Res.* **18**(6), 859–866 (2001).
- <sup>9</sup>A. D. Bond, "Introduction to the special issue on crystal engineering," *Acta Crystallogr., Sect. B: Struct. Sci., Cryst. Eng. Mater.* **70**(1), 1–2 (2014).
- <sup>10</sup>A. M. Reilly, R. I. Cooper, C. S. Adjiman, S. Bhattacharya, A. Daniel Boese, J. G. Brandenburg, P. J. Bygrave, R. Bylsma, J. E. Campbell, R. Car, D. H. Case, R. Chadha, J. C. Cole, K. Cosburn, H. M. Cuppen, F. Curtis, G. M. Day, R. A. DiStasio, Jr., A. Dzyabchenko, B. P. van Eijck, D. M.

- Elking, J. A. van den Ende, J. C. Facelli, M. B. Ferraro, L. Fusti-Molnar, C.-A. Gatsiou, T. S. Gee, R. de Gelder, L. M. Ghiringhelli, H. Goto, S. Grimme, R. Guo, D. W. M. Hofmann, J. Hoja, R. K. Hylton, L. Iuzzolino, W. Jankiewicz, D. T. de Jong, J. Kendrick, N. J. J. de Klerk, H.-Y. Ko, L. N. Kuleshova, X. Li, S. Lohani, F. J. J. Leusen, A. M. Lund, J. Lv, Y. Ma, N. Marom, A. E. Masunov, P. McCabe, D. P. McMahon, H. Meeke, M. P. Metz, A. J. Misquitta, S. Mohamed, B. Monserrat, R. J. Needs, M. A. Neumann, J. Nyman, S. Obata, H. Oberhofer, A. R. Oganov, A. M. Orendt, G. I. Pagola, C. C. Pantelides, C. J. Pickard, R. Podeszwa, L. S. Price, S. L. Price, A. Pulido, M. G. Read, K. Reuter, E. Schneider, C. Schober, G. P. Shields, P. Singh, I. J. Sugden, K. Szalewicz, C. R. Taylor, A. Tkatchenko, M. E. Tuckerman, F. Vacarro, M. Vasileiadis, A. Vazquez-Mayagoitia, L. Vogt, Y. Wang, R. E. Watson, G. A. de Wijs, J. Yang, Q. Zhu, and C. R. Groom, "Report on the sixth blind test of organic crystal structure prediction methods," *Acta Crystallogr., Sect. B: Struct. Sci., Cryst. Eng. Mater.* **72**(4), 439–459 (2016).
- <sup>11</sup>J. D. Dunitz and H. A. Scheraga, "Exercises in prognostication: Crystal structures and protein folding," *Proc. Natl. Acad. Sci. U. S. A.* **101**(40), 14309–14311 (2004).
- <sup>12</sup>A. Laio and M. Parrinello, "Escaping free-energy minima," *Proc. Natl. Acad. Sci. U. S. A.* **99**(20), 12562–12566 (2002).
- <sup>13</sup>R. Martoák, A. Laio, and M. Parrinello, "Predicting crystal structures: The Parrinello-Rahman method revisited," *Phys. Rev. Lett.* **90**(7), 075503 (2003).
- <sup>14</sup>R. Martoák, A. Laio, M. Bernasconi, C. Ceriani, P. Raiteri, F. Zipoli, and M. Parrinello, "Simulation of structural phase transitions by metadynamics," *Z. Kristallogr. - Cryst. Mater.* **220**(5/6), 1–11 (2005).
- <sup>15</sup>R. Martoák, D. Donadio, A. R. Oganov, and M. Parrinello, "From four- to six-coordinated silica: Transformation pathways from metadynamics," *Phys. Rev. B* **76**(1), 014120 (2007).
- <sup>16</sup>C. Ceriani, A. Laio, E. Fois, A. Gamba, R. Martoák, and M. Parrinello, "Molecular dynamics simulation of reconstructive phase transitions on an anhydrous zeolite," *Phys. Rev. B* **70**(11), 113403 (2004).
- <sup>17</sup>F. Zipoli, M. Bernasconi, and R. Martoák, "Constant pressure reactive molecular dynamics simulations of phase transitions under pressure: The graphite to diamond conversion revisited," *Eur. Phys. J. B* **39**(1), 41–47 (2004).
- <sup>18</sup>P. G. Karamertzanis, P. Raiteri, M. Parrinello, M. Leslie, and S. L. Price, "The thermal stability of lattice-energy minima of 5-fluorouracil: Metadynamics as an aid to polymorph prediction," *J. Phys. Chem. B* **112**(14), 4298–4308 (2008).
- <sup>19</sup>P. Raiteri, R. Martoák, and M. Parrinello, "Exploring polymorphism: The case of benzene," *Angew. Chem., Int. Ed.* **44**(24), 3769–3773 (2005).
- <sup>20</sup>T. Lukinov, A. Rosengren, R. Martoák, and A. B. Belonoshko, "A metadynamics study of the *fcc*–*bcc* phase transition in Xenon at high pressure and temperature," *Comput. Mater. Sci.* **107**, 66–71 (2015).
- <sup>21</sup>T.-Q. Yu and M. E. Tuckerman, "Temperature-accelerated method for exploring polymorphism in molecular crystals based on free energy," *Phys. Rev. Lett.* **107**(1), 015701 (2011).
- <sup>22</sup>T.-Q. Yu, P.-Y. Chen, M. Chen, A. Samanta, E. Vanden-Eijnden, and M. Tuckerman, "Order-parameter-aided temperature-accelerated sampling for the exploration of crystal polymorphism and solid-liquid phase transitions," *J. Chem. Phys.* **140**(21), 214109 (2014).
- <sup>23</sup>E. Schneider, L. Vogt, and M. E. Tuckerman, "Exploring polymorphism of benzene and naphthalene with free energy based enhanced molecular dynamics," *Acta Crystallogr., Sect. B: Struct. Sci., Cryst. Eng. Mater.* **72**(4), 542–550 (2016).
- <sup>24</sup>F. Datchi, V. M. Giordano, P. Munsch, and A. Marco Saitta, "Structure of carbon dioxide phase IV: Breakdown of the intermediate bonding state scenario," *Phys. Rev. Lett.* **103**(18), 185701 (2009).
- <sup>25</sup>F. Datchi, B. Mallick, A. Salamat, and S. Ninet, "Structure of polymeric carbon dioxide CO<sub>2</sub>-V," *Phys. Rev. Lett.* **108**(12), 125701 (2012).
- <sup>26</sup>M. Santoro and F. A. Gorelli, "High pressure solid state chemistry of carbon dioxide," *Chem. Soc. Rev.* **35**(10), 918 (2006).
- <sup>27</sup>C. S. Yoo, H. Cynn, F. Gygi, G. Galli, V. Iota, M. Nicol, S. Carlson, D. Häusermann, and C. Mailhot, "Crystal structure of carbon dioxide at high pressure: Superhard polymeric carbon dioxide," *Phys. Rev. Lett.* **83**(26), 5527–5530 (1999).
- <sup>28</sup>C. S. Yoo, H. Kohlmann, H. Cynn, M. F. Nicol, V. Iota, and T. LeBihan, "Crystal structure of pseudo-six-fold carbon dioxide phase II at high pressures and temperatures," *Phys. Rev. B* **65**(10), 104103 (2002).
- <sup>29</sup>J.-H. Park, C. S. Yoo, V. Iota, H. Cynn, M. F. Nicol, and T. Le Bihan, "Crystal structure of bent carbon dioxide phase IV," *Phys. Rev. B* **68**(1), 014107 (2003).

- <sup>30</sup>C.-S. Yoo, "Physical and chemical transformations of highly compressed carbon dioxide at bond energies," *Phys. Chem. Chem. Phys.* **15**(21), 7949 (2013).
- <sup>31</sup>V. M. Giordano and F. Datchi, "Molecular carbon dioxide at high pressure and high temperature," *Europhys. Lett.* **77**(4), 46002 (2007).
- <sup>32</sup>V. Iota and C.-S. Yoo, "Phase diagram of carbon dioxide: Evidence for a new associated phase," *Phys. Rev. Lett.* **86**(26), 5922–5925 (2001).
- <sup>33</sup>F. Datchi, G. Weck, A. M. Saitta, Z. Raza, G. Garbarino, S. Ninet, D. K. Spaulding, J. A. Queyroux, and M. Mezouar, "Structure of liquid carbon dioxide at pressures up to 10 GPa," *Phys. Rev. B* **94**(1), 014201 (2016).
- <sup>34</sup>V. Iota, C.-S. Yoo, J.-H. Klepeis, Z. Jenei, W. Evans, and H. Cynn, "Six-fold coordinated carbon dioxide VI," *Nat. Mater.* **6**(1), 34–38 (2007).
- <sup>35</sup>S. R. Shieh, I. Jarrige, M. Wu, N. Hiraoka, J. S. Tse, Z. Mi, L. Kaci, J.-Z. Jiang, and Y. Q. Cai, "Electronic structure of carbon dioxide under pressure and insights into the molecular-to-nonmolecular transition," *Proc. Natl. Acad. Sci. U. S. A.* **110**(46), 18402–18406 (2013).
- <sup>36</sup>K. Aoki, H. Yamawaki, M. Sakashita, Y. Gotoh, and K. Takemura, "Crystal structure of the high-pressure phase of solid CO<sub>2</sub>," *Science* **263**(5145), 356–358 (1994).
- <sup>37</sup>S. A. Bonev, F. Gygi, T. Ogitsu, and G. Galli, "High-pressure molecular phases of solid carbon dioxide," *Phys. Rev. Lett.* **91**(6), 065501 (2003).
- <sup>38</sup>B. Kuchta and R. D. Eters, "Prediction of a high-pressure phase transition and other properties of solid CO<sub>2</sub> at low temperatures," *Phys. Rev. B* **38**(9), 6265–6269 (1988).
- <sup>39</sup>R. D. Eters and B. Kuchta, "Static and dynamic properties of solid CO<sub>2</sub> at various temperatures and pressures," *J. Chem. Phys.* **90**(8), 4537 (1989).
- <sup>40</sup>B. Kuchta and R. D. Eters, "Generalized free-energy method used to calculate the high-pressure, high-temperature phase transition in solid CO<sub>2</sub>," *Phys. Rev. B* **47**(22), 14691–14695 (1993).
- <sup>41</sup>J. Li, O. Sode, G. A. Voth, and S. Hirata, "A solid-solid phase transition in carbon dioxide at high pressures and intermediate temperatures," *Nat. Commun.* **4**, 2647 (2013).
- <sup>42</sup>S. Hirata, K. Gilliard, X. He, J. Li, and O. Sode, "Ab initio molecular crystal structures, spectra, and phase diagrams," *Acc. Chem. Res.* **47**(9), 2721–2730 (2014).
- <sup>43</sup>F. A. Gorelli, V. M. Giordano, P. R. Salvi, and R. Bini, "Linear carbon dioxide in the high-pressure high-temperature crystalline phase IV," *Phys. Rev. Lett.* **93**(20), 205503 (2004).
- <sup>44</sup>H. Olijnyk, H. Däuffer, H.-J. Jodl, and H. D. Hochheimer, "Effect of pressure and temperature on the Raman spectra of solid CO<sub>2</sub>," *J. Chem. Phys.* **88**(7), 4204–4212 (1988).
- <sup>45</sup>A. Barducci, G. Bussi, and M. Parrinello, "Well-tempered metadynamics: A smoothly converging and tunable free-energy method," *Phys. Rev. Lett.* **100**(2), 020603 (2008).
- <sup>46</sup>B. Peters, "Reaction coordinates and mechanistic hypothesis tests," *Annu. Rev. Phys. Chem.* **67**(1), 669–690 (2016).
- <sup>47</sup>M. E. Tuckerman, *Statistical Mechanics: Theory and Molecular Simulation* (Oxford University Press, 2010).
- <sup>48</sup>A. Barducci, M. Bonomi, and M. Parrinello, "Metadynamics," *Wiley Interdiscip. Rev.: Comput. Mol. Sci.* **1**(5), 826–843 (2011).
- <sup>49</sup>C. Abrams and G. Bussi, "Enhanced sampling in molecular dynamics using metadynamics, replica-exchange, and temperature-acceleration," *Entropy* **16**(1), 163–199 (2013).
- <sup>50</sup>A. Laio and F. L. Gervasio, "Metadynamics: A method to simulate rare events and reconstruct the free energy in biophysics, chemistry and material science," *Rep. Prog. Phys.* **71**(12), 126601 (2008).
- <sup>51</sup>O. Valsson, P. Tiwary, and M. Parrinello, "Enhancing important fluctuations: Rare events and metadynamics from a conceptual viewpoint," *Annu. Rev. Phys. Chem.* **67**(1), 159–184 (2016).
- <sup>52</sup>F. Giberti, M. Salvalaglio, and M. Parrinello, "Metadynamics studies of crystal nucleation," *IUCrJ* **2**(2), 256–266 (2015).
- <sup>53</sup>J. J. Potoff, J. R. Errington, and A. Z. Panagiotopoulos, "Molecular simulation of phase equilibria for mixtures of polar and non-polar components," *Mol. Phys.* **97**(10), 1073–1083 (1999).
- <sup>54</sup>J. J. Potoff and J. Ilja Siepmann, "Vapor-liquid equilibria of mixtures containing alkanes, carbon dioxide, and nitrogen," *AIChE J.* **47**(7), 1676–1682 (2001).
- <sup>55</sup>C. G. Aimoli, E. J. Maginn, and C. R. A. Abreu, "Force field comparison and thermodynamic property calculation of supercritical CO<sub>2</sub> and CH<sub>4</sub> using molecular dynamics simulations," *Fluid Phase Equilib.* **368**, 80–90 (2014).
- <sup>56</sup>G. Perez-Sanchez, D. Gonzalez-Salgado, M. M. Pineiro, and C. Vega, "Fluid-solid equilibrium of carbon dioxide as obtained from computer simulations of several popular potential models: The role of the quadrupole," *J. Chem. Phys.* **138**(8), 084506 (2013).
- <sup>57</sup>S. L. Price, "The structure of the homonuclear diatomic solids revisited," *Mol. Phys.* **62**(1), 45–63 (1987).
- <sup>58</sup>T. Sanghi and N. R. Aluru, "Coarse-grained potential models for structural prediction of carbon dioxide (CO<sub>2</sub>) in confined environments," *J. Chem. Phys.* **136**(2), 024102 (2012).
- <sup>59</sup>G. Bussi, D. Donadio, and M. Parrinello, "Canonical sampling through velocity rescaling," *J. Chem. Phys.* **126**(1), 014101 (2007).
- <sup>60</sup>H. J. C. Berendsen, J. P. M. Postma, W. F. van Gunsteren, A. DiNola, and J. R. Haak, "Molecular dynamics with coupling to an external bath," *J. Chem. Phys.* **81**(8), 3684 (1984).
- <sup>61</sup>M. J. Abraham, D. van der Spoel, E. Lindahl, B. Hess, and GRO-MACS Development Team, GROMACS User Manual version 5.1.1, [www.gromacs.org](http://www.gromacs.org), 2015.
- <sup>62</sup>G. A. Tribello, M. Bonomi, D. Branduardi, C. Camilloni, and G. Bussi, "PLUMED 2: New feathers for an old bird," *Comput. Phys. Commun.* **185**(2), 604–613 (2014).
- <sup>63</sup>W. Humphrey, A. Dalke, and K. Schulten, "VMD: Visual molecular dynamics," *J. Mol. Graphics* **14**, 33–38 (1996).
- <sup>64</sup>M. Salvalaglio, T. Vetter, F. Giberti, M. Mazzotti, and M. Parrinello, "Uncovering molecular details of urea crystal growth in the presence of additives," *J. Am. Chem. Soc.* **134**(41), 17221–17233 (2012).
- <sup>65</sup>M. Salvalaglio, T. Vetter, M. Mazzotti, and M. Parrinello, "Controlling and predicting crystal shapes: The case of urea," *Angew. Chem., Int. Ed.* **52**(50), 13369–13372 (2013).
- <sup>66</sup>M. Salvalaglio, C. Perego, F. Giberti, M. Mazzotti, and M. Parrinello, "Molecular-dynamics simulations of urea nucleation from aqueous solution," *Proc. Natl. Acad. Sci. U. S. A.* **112**(1), E6–E14 (2015).
- <sup>67</sup>F. Giberti, M. Salvalaglio, M. Mazzotti, and M. Parrinello, "Insight into the nucleation of urea crystals from the melt," *Chem. Eng. Sci.* **121**, 51–59 (2015).
- <sup>68</sup>A. Berteotti, A. Barducci, and M. Parrinello, "Effect of urea on the  $\beta$ -Hairpin conformational ensemble and protein denaturation mechanism," *J. Am. Chem. Soc.* **133**(43), 17200–17206 (2011).
- <sup>69</sup>A. Samanta, M. E. Tuckerman, T.-Q. Yu, and E. Weinan, "Microscopic mechanisms of equilibrium melting of a solid," *Science* **346**(6210), 729–732 (2014).
- <sup>70</sup>M. Forsblom and G. Grimvall, "How superheated crystals melt," *Nat. Mater.* **4**(5), 388 (2005).
- <sup>71</sup>G. C. Sosso, J. Chen, S. J. Cox, M. Fitzner, P. Pedevilla, A. Zen, and A. Michaelides, "Crystal nucleation in liquids: Open questions and future challenges in molecular dynamics simulations," *Chem. Rev.* **116**(12), 7078–7116 (2016).
- <sup>72</sup>M. Bonomi, A. Barducci, and M. Parrinello, "Reconstructing the equilibrium Boltzmann distribution from well-tempered metadynamics," *J. Comput. Chem.* **30**(11), 1615–1621 (2009).